

Bak-Tang-Wiesenfeld model in the upper critical dimension: Induced criticality in lower-dimensional subsystems

H. Dashti-Naserabadi^{1,*} and M. N. Najafi^{2,†}

¹*Physics and Accelerators Research School, NSTRI, AEOI 11365-3486, Tehran, Iran*

²*Department of Physics, University of Mohaghegh Ardabili, P.O. Box 179, Ardabil, Iran*

(Received 25 July 2017; revised manuscript received 20 September 2017; published 9 October 2017)

We present extensive numerical simulations of Bak-Tang-Wiesenfeld (BTW) sandpile model on the hypercubic lattice in the upper critical dimension $D_u = 4$. After re-extracting the critical exponents of avalanches, we concentrate on the three- and two-dimensional (2D) cross sections seeking for the induced criticality which are reflected in the geometrical and local exponents. Various features of finite-size scaling (FSS) theory have been tested and confirmed for all dimensions. The hyperscaling relations between the exponents of the distribution functions and the fractal dimensions are shown to be valid for all dimensions. We found that the exponent of the distribution function of avalanche mass is the same for the d -dimensional cross sections and the d -dimensional BTW model for $d = 2$ and 3. The geometrical quantities, however, have completely different behaviors with respect to the same-dimensional BTW model. By analyzing the FSS theory for the geometrical exponents of the two-dimensional cross sections, we propose that the 2D induced models have degrees of similarity with the Gaussian free field (GFF). Although some local exponents are slightly different, this similarity is excellent for the fractal dimensions. The most important one showing this feature is the fractal dimension of loops d_f , which is found to be $1.50 \pm 0.02 \approx \frac{3}{2} = d_f^{\text{GFF}}$.

DOI: [10.1103/PhysRevE.96.042115](https://doi.org/10.1103/PhysRevE.96.042115)

I. INTRODUCTION

The concept of self-organized criticality was introduced by Bak, Tang, and Wiesenfeld [1,2] (BTW model) and was realized with the so-called Abelian sandpile model. Many analytical and theoretical aspects of this model in any Euclidean dimensions is known [3–7]. Among them, one can mention different height and cluster probabilities [8], avalanche distribution [9–11], the connection of the model to spanning trees [12], ghost models [13], and q -state Potts model [14,15]. For a good review, see Ref. [16].

The critical properties of the sandpile models on their upper critical dimension D_u is a challenging problem in this context [4]. It is known that $D_u = 4$ for BTW model [4,6,17], whereas for other variants of sandpile model it may be different; e.g., the dissipative sandpile model was conjectured to be $D_u^{\text{dissipative}} = 5$ [18]. Though the critical exponents of the model on the higher spatial dimensions are expected to be the same as the mean-field one [11], the behaviors right at the upper critical dimension are more complex and are shown to be logarithmically corrected [19,20]. Apart from this complexity, there is a theoretical interest on the problem of energy propagation in lower dimensional portions of this system [21]. More explicitly, the question is whether the exponents of the avalanches in the lower-dimensional subsystems are the same as the mean-field ones [21]. This reveals the internal structure of the original model [22], which is the BTW model in the upper critical dimension in this paper.

A common way to lower the dimensionality of the system is the use of cross sections; i.e., track the avalanches in the cross sections of the model in hand [21,22]. In this way, we

will have an effective $(d - 1)$ -dimensional model which has the effect of the extra (d th) dimension whose information is coded in the effective $(d - 1)$ -dimensional model. This yields some valuable information about the original (d -dimensional) system. This helps to observe how things change when the dimensionality of the system is lowered in the presence of the d th dimension and how the criticality of the original model affects the mentioned subsystem [22]. This is more vital for $d = D_u = 4$ for BTW model, since this dimension is the margin between non-mean-field and mean-field behaviors and one can observe how things change when the *effective* dimension of the system is lowered and how far the resulting exponents will be from the mean field results. This needs large scale numerical simulations and high-quality data, since as a well-known fact the numerical exponents of the sandpile models is a challenging problem.

In this paper, we present a detailed analysis of the problem; After reproducing the results of the previous works on the BTW model in four-dimensional (4D) systems [4], we take into account the effective three-dimensional (3D) system by considering a cubic cross section at $x_1 = L/2$ (in which x_1 is the arbitrary dimension to be subtracted and L is the linear size of the lattice). We will see that the finite-size scaling theory is applicable for both $d = 4$ (as expected) and effective $d = 3$ models. Interestingly, some calculated exponents (not all) are identical to the 3D BTW model. The other effective model is obtained by further reducing the dimensionality of the system, i.e., the model living in $x_1 = x_2 = L/2$ cross section. We will see that the resulting induced model is very different from both mean-field theory and two-dimensional (2D) BTW model. The justification of hyperscaling relations between exponents shows that the resulting system satisfies the finite-scaling relations. At the end, the geometrical aspects of the loops in 2D is analyzed, showing that the fractal dimension of loops is nearly 1.5, which is consistent with the Gaussian free field (GFF) [23–27].

*h.dashti82@gmail.com

†morteza.nattagh@gmail.com

The paper has been organized as follows: In Sec. II, we introduce and describe the model and determine the effective models. In Sec. III, we present the results and some findings of the previous works reproduced for the four-dimensional case. The results for effective three dimensions and two dimensions are presented in Sec. III A and Sec. III B, respectively. Section IV is devoted to a comprehensive conclusion.

II. MODEL AND SIMULATIONS

In this section, we briefly introduce the standard BTW model on d -dimensional hypercubic lattice [1]; each site i has an integer height (energy) $h_i \geq 1$. At initial state, one can set randomly the height of each site in which $h_i \leq h_c$. h_c is the threshold height equal to the number of nearest neighbors of each site (e.g, for hypercubic lattice $h_c = 2d$). At each time step a grain is added on a randomly chosen site ($h_i \rightarrow h_i + 1$). If the height of this site exceeds h_c , a toppling occurs: $h_i \rightarrow h_i + \Delta_{i,j}$ in which $\Delta_{i,j} = -h_c$ if $i = j$, $\Delta_{i,j} = 1$ if i and j are neighbors, and zero otherwise. A toppling can cause the nearest-neighbor sites to become unstable (have height higher than h_c) and topple on their turn and so on, until all of the lattice sites are below the critical threshold (stable state). This process is called an avalanche. The model is conservative and energy is dissipated only from the boundary sites. The properties of the model in $d = 2$ has been investigated extensively and well understood in the literature [16,28,29], as well as $d = 3$ [4,11,21]. For $d = 5,6$ and higher dimensions, the exponents are consistent with the mean-field results [4,30]. The upper critical dimension that separates these two phases is $d = D_u = 4$, in which the determination of the exponents needs some cares [4,19].

One way to recognize the critical systems is by the power-law behaviors and the emergence of critical exponents. Let Ω denote the total (host) system and $\omega \subset \Omega$ is some subsystem of Ω . A very important question is whether the criticality of Ω can induce critical (such as power-law) behaviors in ω as its subsystem. This problem is relevant since we are sometimes

interested in the models that live on the hypersurfaces. If the subsystem ω also enjoys the criticality as the host model, we name it as the *induced criticality*. The induced critical subsystem ω may show very different properties with respect to the critical (host) model [21]. This is due to the fact that in the dynamics of ω , some information spreads out toward the host Ω , and vice versa, which causes the correlations in ω to differ from both host Ω as well as *isolated* model in ω (isolated model means that the subsystem ω is not embedded in any larger system). This problem can be realized in lower dimensional cross sections of d -dimensional (host) system. The important question is how the information in d dimensions would be reflected to the lower dimensions. In this mechanism, one can measure how some information is lost and how the degrees of freedom in the subtracted dimension affect the lower dimensional model, i.e., which model lives in the lowered dimensional system. If the subtracted dimension is temporal, then one is looking at a *frozen* model with no dynamics. The investigation of the contour lines of statistical systems [31] and ground state of the quantum systems [32] are some examples. A more interesting situation is the case in which the subtracted dimension is spatial one. The example is the cross sections of 3D BTW model, which is proposed to share some critical behaviors as the 2D Ising model [21]. In this paper, along with the four-dimensional BTW (as the host) model, we consider the two- and three-dimensional cross-sections as the mentioned subsystems. The effective two and three-dimensional energy propagation for the BTW model is the aim of the present paper. We directly map a $d = 4$ -dimensional system to $d - 1 = 3$ and $d - 2 = 2$ -dimensional one by using cross sections. The induced criticality of the resulting system is shown to be completely different from the four-dimensional case. A schematic set up of this process has been presented in Fig. 1(a), in which shows a cross section of the hypercubic lattice at $x_1 = L/2$. In this figure, the colored small boxes are the sites in which a toppling occurred in an avalanche. Apparently, this cross section is a three-dimensional system with some colored and uncolored sites which is analyzed in this paper. The $d - 2$ effective model is defined on

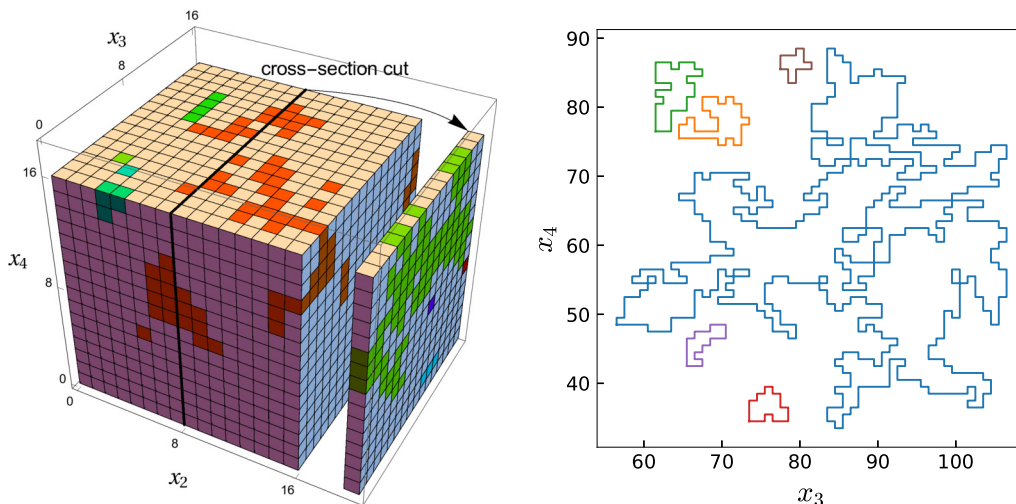


FIG. 1. (a) The avalanche region of 3D cross section of a 4D avalanche on a hypercubic lattice with size $L = 16$, and also a cut from its 2D cross section. (b) The boundary loop of an avalanche of 2D cross section of a 4D avalanche on a hypercubic lattice with size $L = 144$.

$x_1 = x_2 = L/2$ cross sections which is apparently two-dimensional system [see Fig. 1(a)]. For this case, in addition to customary investigations, we have also studied the geometrical aspects, like the closed loops which is defined as the external frontier of a connected avalanche [see Fig. 1(b)]. Note that though the original avalanche is simply connected, in the three and two-dimensional effective models, it can be composed of some disjoint components. An example has been shown in

Fig. 1(a), in which different components have been shown by different colors (in this figure the subtracted dimensions have been considered to be x_1 and x_2). The first attempt concerning the SOC systems was made by Dashti-Naseabadi *et al.* [21], in which two-dimensional propagation of three-dimensional BTW model was investigated.

In the following sections, we analyze global and local properties of this model in 4D, effective 3D and effective 2D

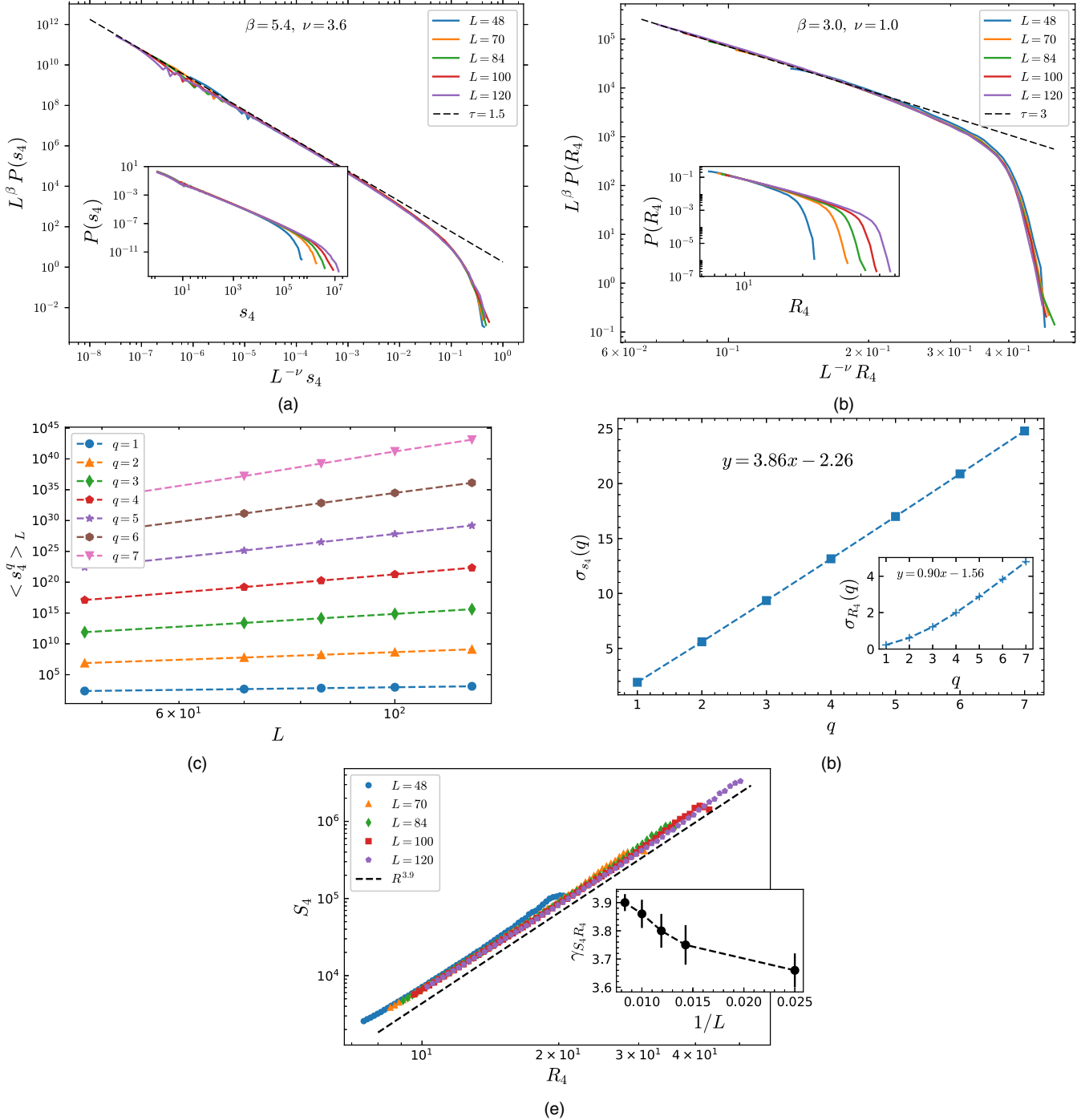


FIG. 2. The distribution function of (a) the number of relaxation events s_4 (which is equivalent to size of avalanche S_4), with the exponent $\tau_{s_4} = 1.50(3)$ (derived using χ^2 method), and (b) the gyration radius R_4 with the exponent $\tau_{R_4} = 3.00(4)$. (c) The q th moment of s_4 versus different sizes L . (d) The exponent σ_{s_4} versus q , which is derived from Eq. (3). Inset: The exponent σ_{R_4} versus q . (e) The function S_4 versus R_4 with slope (fractal dimension) $\gamma_{S_4 R_4}^{L=120} = 3.90(3)$. Inset: the finite-size effect for $\gamma_{S_4 R_4}^\infty = 4.00(5)$.

systems. Our analysis for 4D avalanches involves the scaling relation between the global quantities and their distribution functions, as well as local ones. The quantities studied in this paper are as follows ($d = 2, 3$, and 4 shows the dimension): the number of relaxation events s_d , the size (mass) of the connected component of an avalanche S_d , the number of distinct toppled lattice sites sd_d , the gyration radius R_d which is defined as: $R_d^2 \equiv \frac{1}{S_d} \sum_{i=1}^{S_d} (\vec{r}_i - \vec{r}_{\text{com}})^2$, which is the gyration radius of the points involved in a connected component of an avalanche. In this formula, \vec{r}_i is the position vector of the i th point of the avalanche in d spatial dimension and $\vec{r}_{\text{com}} \equiv \frac{1}{S_d} \sum_{i=1}^{S_d} \vec{r}_i$ is the center of mass of the avalanche.

Note that s_d, sd_d are the same; since the probability that a site topples more than one time in an avalanche is negligibly small for $d \geq 3$ [33]. Moreover, S_d is equal to s_d and sd_d in $d = 4$, since the avalanches are simply connected, but it is not true for cross sections; because an avalanche may have multiple distinct components in the cross sections. For the two-dimensional case, we have also analyzed the following geometrical quantities: the loop lengths l , which is the length of the loop that is the external perimeter of a 2D cross section of a micro avalanche; the area inside loops a , which is the total area that is contained in the loop; the gyration radius of loops r .

Let us mention some comments concerning the distribution functions of the statistical observables. For any critical system in the thermodynamic limit $L \rightarrow \infty$, one expects that the distribution function of any statistical observable x (=one of the observables of the above list) behaves like $P(x) \sim x^{-\tau_x}$ in which τ_x is the exponent corresponding to the observable $x = s_d, sd_d, S_d, R_d$ with $d = 4, 3, 2$ and also l, a , and r .

An important relation is for the fractal dimensions defined by $y \sim x^{\gamma_{xy}}$ in which y and x are the statistical observables. The relation $P_x(x)dx = P_y(y)dy$ for the corresponding distribution functions then leads to the scaling relation,

$$\gamma_{xy} = \frac{\tau_y - 1}{\tau_x - 1}. \tag{1}$$

It is notable that this is the case only when the conditional probability $P(x|y)$ be a narrow function of both x and y .

For finite systems, the finite-size scaling theory predicts that [4]

$$P(x, L) = L^{-\beta} g(xL^{-\nu_x}), \tag{2}$$

in which g is a universal function and β and ν are the exponents corresponding to x . A simple dimensional analysis shows that $\tau_x = \frac{\beta}{\nu}$, which will be tested for all observables in the remainder of the paper. The exponent ν_x determines the cutoff behavior of the probability distribution function. If finite-size scaling works, all distributions $P_x(x, L)$ for various system sizes have to collapse, including their cutoffs. Then the argument of the universal function g has to be constant. One can simply show that $r_{\text{cutoff}} \sim L^\nu$; i.e., the cutoff radius should scale with the system size L and finally one gets $\nu_x = \gamma_{xr}$ [4].

The monofractality and multifractality of the sandpile models is the notion that is served as an important issue in the literature. Before closing the section, we mention some points on the multifractal structure of the model, which is a longstanding debate in the literature. In fact, the relation Eq. (2) is only correct for monofractal systems. To investigate this, we use

the method of moment analysis presented in Ref. [34]. To this end, we should calculate the q th moment of the x variable $\langle x^q \rangle$ ($x =$ the statistical observable in each dimension), defined by

$$\langle x^q \rangle_L = \int P_x(x, L)x^q dx \sim L^{\sigma_x(q)}, \tag{3}$$

in which $\sigma_x(q) = \nu_x(q - \tau_x + 1)$ for monofractal systems. It is seen that for monofractal systems $\sigma_x(q)$ has the linear behavior in terms of q , i.e., $\sigma_x(q + 1) - \sigma_x(q) = \nu_x$. It is a very serious test for monofractality and multifractality of the system. In addition, the exponents can be extracted from this analysis. In the following sections, we use this analysis.

III. NUMERICAL RESULTS

This section is devoted to the numerical results. We present the results for four-, three-, and two-dimensional cases separately. To extract the exponents, we have used the data collapse technique. To fit the data, we have used the χ -square method. The results for all dimensions show a clean finite-size scaling with the exponents to be reported in the following sections. As stated in the previous section, the statistics of s_d and sd_d is the same and we only consider s_d in the following sections.

We consider four-dimensional BTW model on a hypercubic lattice of linear sizes $L = 48, 70, 84, 100$, and 120 , and its three- and two-dimensional cross sections. For calculating our desired quantities, more than 5×10^7 avalanches are taken into account. We start with a random height distribution $h_i \in [1, 6]$ and inject the sand grains randomly through the sample. Once the system reached the steady state, the statistical observables are analyzed. To make the samples independent, L^2 random injections are made between two successive samplings.

First, we have reproduced the results of the previous works. These results have been gathered in Figs. 2(a), 2(b), and 2(e). In Fig. 2(a), the data collapse of the distribution function of s_4 has been shown for various lattice sizes. Our analysis shows that this function fulfills properly the finite-size scaling hypothesis, Eq. (2), with $\beta_{s_4} = 5.4$, $\nu_{s_4} = 3.6$, and $\tau_{s_4} = 1.50(3)$. These results are consistent with the mean-field ones [4] as indicated in Table I. In Fig. 2(b), we see that $\beta_{R_4} = 3.0$, $\nu_{R_4} = 1.0$, and $\tau_{R_4} = 3.00(4)$.

The exponent $\sigma_{s_4}(q)$ has been plotted in Figs. 2(c) and 2(d). In Fig. 2(c), $\langle s_4^q \rangle$ has been calculated in terms of L for various amounts of q . The corresponding $\sigma_{s_4}(q)$ has been shown in the right figure whose slope is $3.86(1)$, which is approximately compatible with $\nu_{s_4} \approx 3.6$. On the other hand, τ_{s_4} can be extracted from this figure to be $1.58(1)$, which is in agreement with the obtained result from data collapsing. The linear behavior of this quantity shows its monofractal behavior. ν_{R_4} and τ_{R_4} have also been reported in the inset of this figure, from which (considering only the linear part of the graph) we see that

TABLE I. The exponents of four-dimensional BTW [4,33] model.

| | τ | ν | β | $\frac{\beta}{\nu}$ | τ_{MF} | ν_{MF} | β_{MF} |
|-------|---------|--------|---------|---------------------|--------------------|-------------------|---------------------|
| s_4 | 1.50(3) | 3.6(1) | 5.4(1) | 1.5 | $\frac{3}{2}$ | 4 | 6 |
| R_4 | 3.00(4) | 1.0(1) | 3.0(1) | 3.0 | — | — | — |

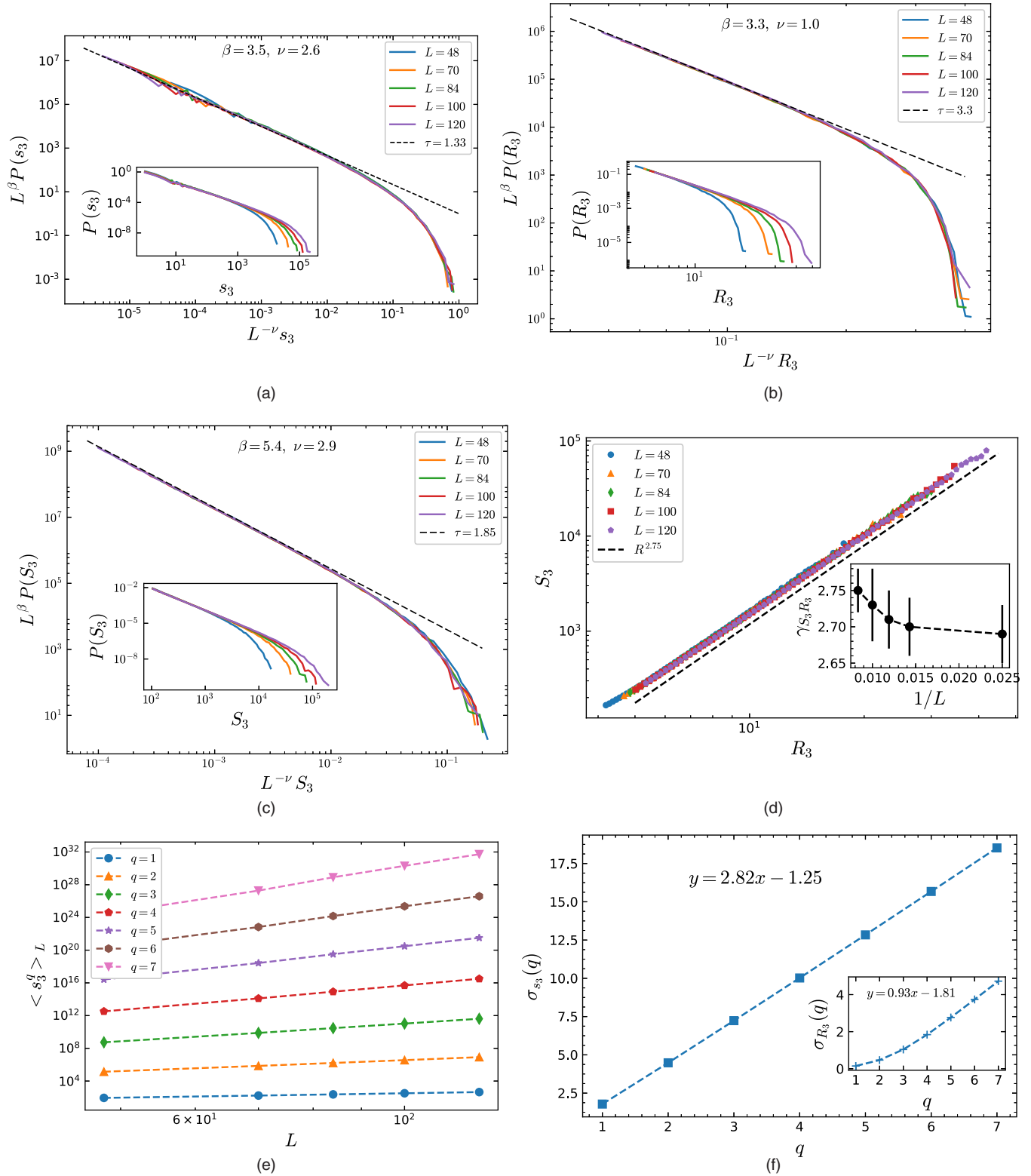


FIG. 3. The distribution function of (a) the number of relaxation events s_3 with the exponent $\tau_{s_3} = 1.33(3)$, (b) the gyration radius R_3 with the exponent $\tau_{R_3} = 3.30(4)$, and (c) the size of the clusters S_3 with the exponent $\tau_{S_3} = 1.85(4)$. (d) The function S_3 versus R_3 with slope (fractal dimension) $\gamma_{S_3 R_3}^{L=120} = 2.75(3)$. Inset: the finite-size effect of $\gamma_{S_3 R_3}$ with $\gamma_{S_3 R_3}^\infty = 2.80(5)$. (e) The q th moment of s_3 versus different sizes L . (f) The exponent σ_{s_3} versus q , which is derived from Eq. (3). Inset: The exponent σ_{R_3} versus q .

$\nu_{R_4} = 0.90(7)$ and $\tau_{R_4} = 2.73(7)$. It is seen that for small q values this graph is not linear, whereas for higher amounts of q the graph shows linear behavior. Such a behavior has also been seen in two-dimensional systems for which considering only the linear part of the graph yields the desired results [35].

The mono- and multifractality of the avalanches in the BTW is a long-standing problem in the literature [11,34]. As pointed out in Ref. [34], the number of topplings (s) shows multifractal behaviors for two dimensions, whereas the mass of the avalanches (S) is monofractal. In four dimensions, the statistics of s and M is the same and as is seen in our analysis, both show the monofractal behaviors.

To measure the fractal dimension of the four-dimensional clusters $\gamma_{S_4 R_4}$, we calculate average S_4 in terms of R_4 , which has been indicated in Fig. 2(e). The measured fractal dimension 3.90(3) for the maximum lattice size $L = 120$ is consistent with the hyperscaling relation 1, i.e., $(\tau_{R_4} - 1)/(\tau_{S_4} - 1) = 4$. For all fractal dimensions we have calculated the finite-size effect and observed that they fulfill the following relation: via the relation all

$$\gamma_{xy} = \gamma_{xy}^{\infty} - \kappa_{xy} \left(\frac{10}{L} \right), \quad (4)$$

in which γ_{xy}^{∞} is the extrapolated exponent (the thermodynamical limit of the exponent, i.e., $L \rightarrow \infty$) and the slope κ_{xy} is another exponent showing the rate of approach to the thermodynamic limit (the factor 10 is to make number more convenient). This has been shown in the inset of the Fig. 2(e), which shows that $\gamma_{S_4 R_4}^{\infty} = 4.0(1)$ and $\kappa_{S_4 R_4} = 2.5$ (the slope has been obtained excluding the bad data for $L = 48$). It is a well-known result in the field [4], i.e., $\gamma_{S_d R_d} = d$ in the d -dimensional BTW model, since the avalanches are simply connected. This is not necessarily true for lower-dimensional cross sections (as will be seen in the following sections), for which the avalanches contain some hollows (untoppled sites), which affect their fractal dimensions.

A. Three dimensions

As stated in the previous section, we measure the induced criticality in lower-dimensional cross sections of the four-dimensional BTW (host) model. This part is devoted to the quantities that are derived from the three-dimensional cross sections that were introduced in Sec. II. We have first extracted the four-dimensional avalanches and then simply have analyzed the three-dimensional cross sections of the avalanches. The results for distribution functions have been shown in Figs. 3(a)–3(c), whose exponents have been gathered in Table II. It is interestingly seen that s_3 has the same exponents as the ones for s in the three-dimensional BTW

TABLE II. The exponents of the three-dimensional cross sections. The exponents for three-dimensional BTW [4,33] model have been shown for comparison.

| | τ | ν | β | $\frac{\beta}{\nu}$ | $\tau_{3\text{DBTW}}$ | $\nu_{3\text{DBTW}}$ | $\beta_{3\text{DBTW}}$ |
|-------|---------|--------|---------|---------------------|-----------------------|----------------------|------------------------|
| s_3 | 1.33(4) | 2.6(1) | 3.5(1) | 1.34 | $\frac{4}{3}$ | 3 | 4 |
| R_3 | 3.30(4) | 1.0(1) | 3.3(1) | 3.3 | 2 | — | — |
| S_3 | 1.85(4) | 2.9(1) | 5.4(1) | 1.86 | $\frac{4}{3}$ | — | — |

model. For example, observe that $\tau_{s_3} = 1.33(4)$, which is consistent with $\tau_s^{\text{3DBTW}} = \frac{4}{3}$ [4]. Although this is true for τ_{s_3} , ν_{s_3} , and β_{s_3} , the results for R_3 and S_3 differ significantly from the 3D BTW model. This shows that the statistics of the total projected avalanche is just like the three-dimensional BTW avalanche, but each individual component of avalanche behaves differently. The other observation is that ν_{R_3} is nearly unity. In fact, as we will see in the next section, this exponent is nearly equal to unity for all cross sections with all definitions of gyration radius. This confirms that the cutoff value of gyration radius (R_{cut}) scales linearly with the system size L for all dimensions which is one of the measures of criticality.

$\gamma_{S_3 R_3}$ and its finite-size relation has been shown in Fig. 3(d) and its inset. From this figure we see that it satisfies the relation 4 with $\gamma_{S_3 R_3}^{\infty} = 2.8$ and $\kappa_{S_3 R_3} = 0.84$. This observation has two important consequences: First, note that it fulfills the hyperscaling relation $\gamma_{S_3 R_3} \approx \gamma_{S_3 R_3}^{\text{hyper scaling}} = \frac{\tau_{R_3} - 1}{\tau_{S_3} - 1} = 2.71$. Second, it shows that the avalanches are not simply connected in the three-dimensional cross sections; i.e., there are some hollows inside them that cause the mass of avalanche to be lower than a simply connected region with the fractal dimension 3.

As in the previous section, we calculate the spectrum of s_3 in this part. It has been shown in Figs. 3(e) and 3(f), in which $\langle s_3^q \rangle_L$ has been plotted in terms of L for various amounts of q . As is evident in the right figure, $\sigma_{s_3}(q)$ is linear in terms of q with the slope 2.82(1), which is in agreement with the numerical amount of $\nu_{s_3} \approx 2.6$. The numerical amount of τ_{s_3} can be read from this figure, which is obtained 1.44(1). This is in agreement with the result in Table II. Also, σ_{R_3} has been plotted in the inset with $\nu_{R_3} = 0.93(5)$ and $\tau_{R_3} = 2.94(5)$.

B. Two dimensions

The more interesting features can be found in two dimensions, since our tools for statistical investigations are more various than higher dimensions. In this case, the statistical fluctuations of the observables are more than the ones for higher dimensions as is explicit in Figs 4(a)–4(c). The 2D exponents and their fittings have been shown in these figures and have been gathered in Table III. Except for s_2 , the results of the exponents for two-dimensional cross sections is very different from the 2D BTW model. This can be deduced from the Table III, from which it is seen that $\tau_{s_2} \approx 2\tau_{s_2}$. In the last row of this table, the results for GFF model have been shown. It is seen that this model is more compatible with 2D induced model, although there are some discrepancies. In the Fig. 4(d) the plot of S_2 - R_2 has been sketched whose inset is the finite size dependence of the slope $\gamma_{S_2 R_2}$. This quantity satisfies

TABLE III. The exponents of local quantities in two-dimensional cross sections. The corresponding exponents for two-dimensional BTW and GFF models have also been shown for comparison.

| | τ | ν | β | $\frac{\beta}{\nu}$ | $\tau_{2\text{DBTW}}$ | $\tau_{2\text{DGFF}}$ |
|-------|----------|--------|---------|---------------------|-----------------------|-----------------------|
| s_2 | 1.20(10) | 1.6(1) | 2.0(1) | 1.25 | 1.293 | — |
| R_2 | 3.60(9) | 1.0(1) | 3.6(1) | 3.6 | $\frac{5}{3}$ | 3 |
| S_2 | 2.45(10) | 2.0(1) | 4.8(1) | 2.4 | $\frac{4}{3}$ | $\frac{31}{15}$ |

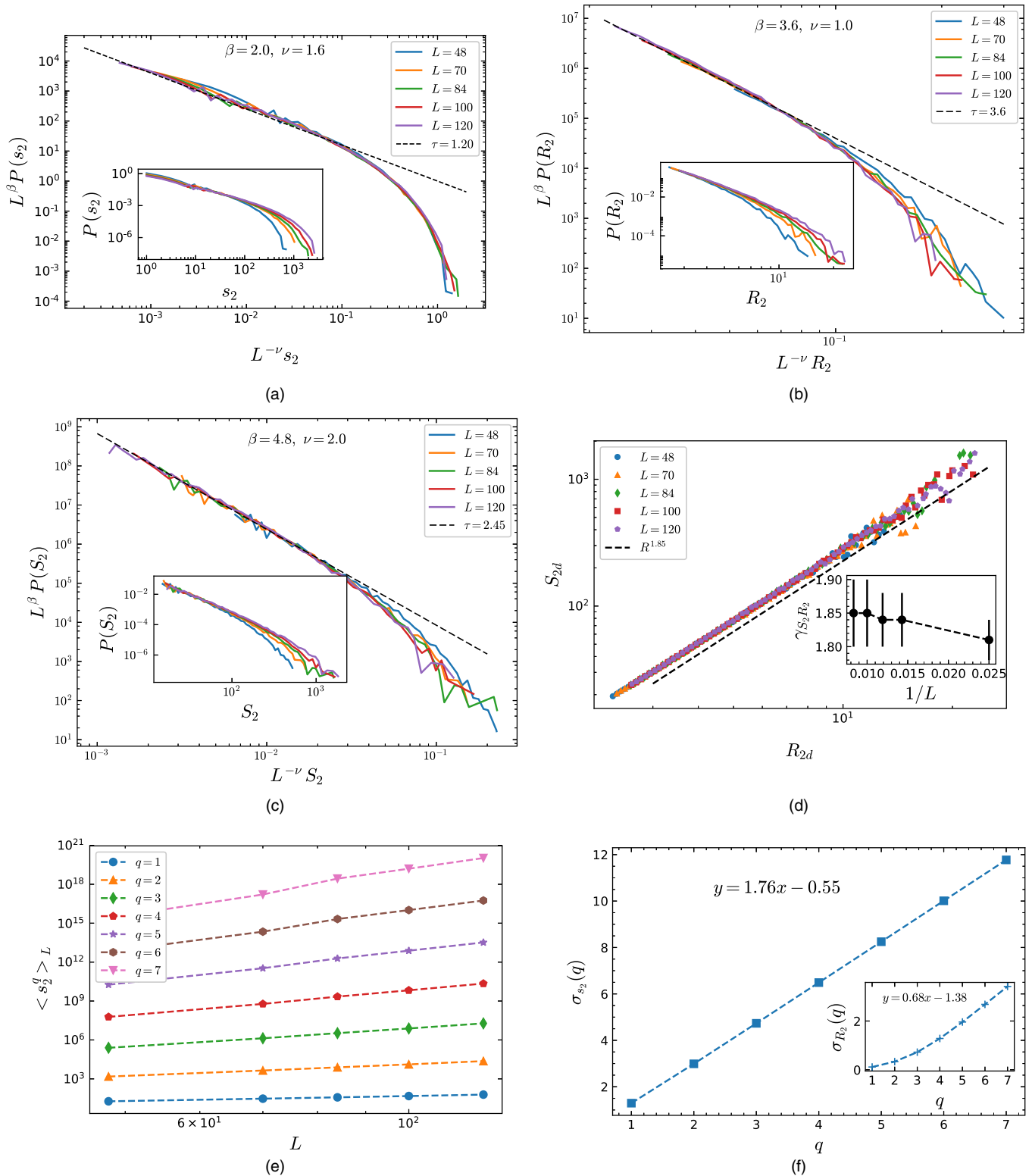


FIG. 4. The distribution function of (a) the number of relaxation events s_2 with the exponent $\tau_{s_2} = 1.20(10)$, (b) the gyration radius R_2 with the exponent $\tau_{R_2} = 3.60(9)$, and (c) the cluster size S_2 with the exponent $\tau_{S_2} = 2.45(10)$. (d) The function S_2 versus R_2 with slope (fractal dimension) $\gamma_{S_2 R_2}^{L=120} = 1.85(5)$. Inset: the finite-size effect of $\gamma_{S_2 R_2}$ with $\gamma_{S_2 R_2}^\infty = 1.86(5)$. (e) The q th moment of s_2 versus different sizes L . (f) The exponent σ_{s_2} versus q , which is derived from Eq. (3). Inset: The exponent σ_{R_2} versus q .

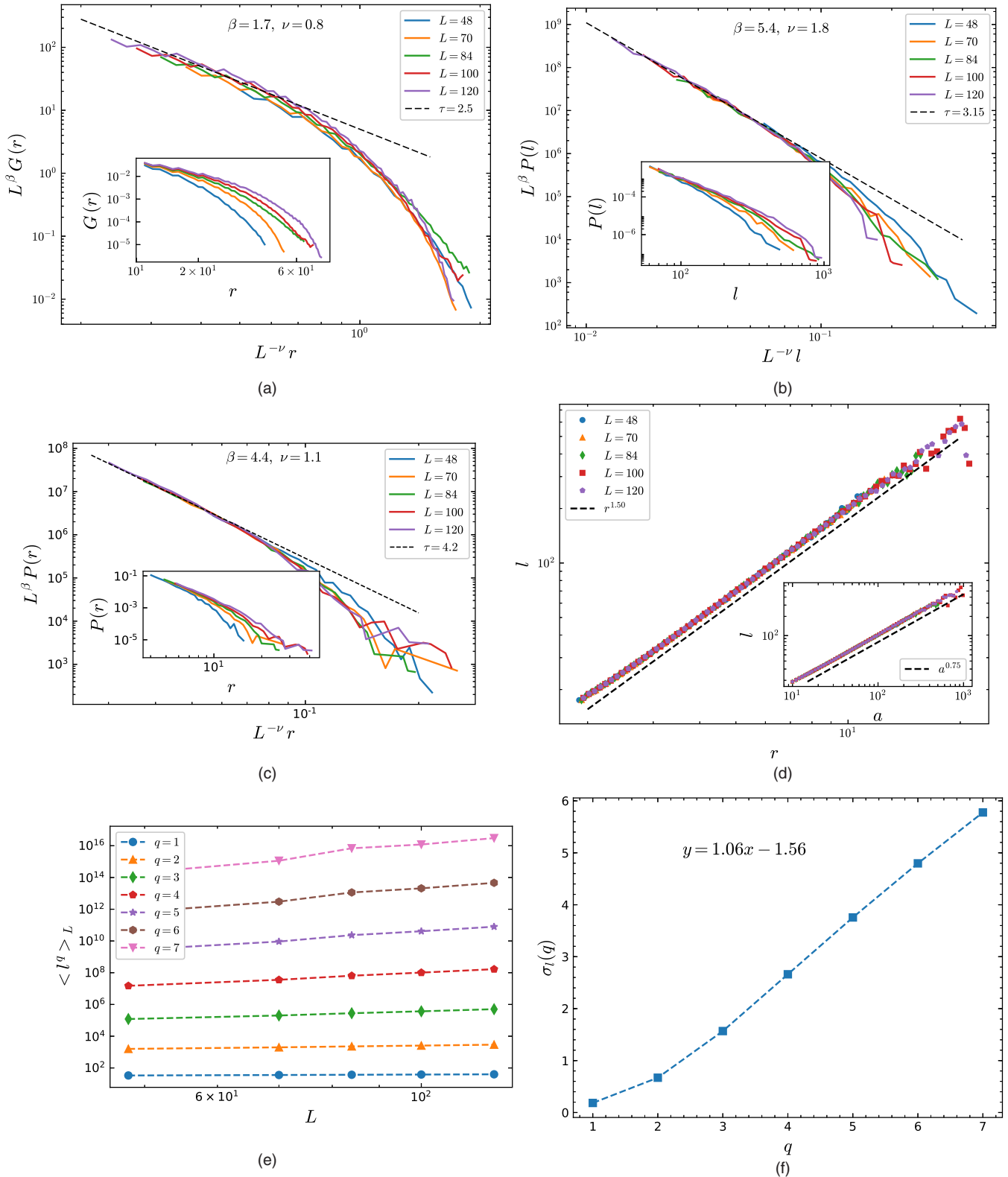


FIG. 5. (a) The Green function in terms of r for various rates of lattice sizes with the exponent $x_l = 2.5(2)$. The distribution function of (b) the length of loops l with the exponent $\tau_l = 3.15(13)$, and (c) the gyration radius r with exponent $\tau_r = 4.20(11)$. (d) The function l versus r with slope (fractal dimension) $\gamma_{rl} = 1.50(2)$. Inset: The function l versus a with slope $\gamma_{al} = 0.75(2)$. (e) The q th moment of l versus different sizes L . (f) The exponent σ_l versus q , which is derived from Eq. (3).

the Eq. (4) as for the higher dimensions. The corresponding exponents are $\gamma_{S_2 R_2}^\infty = 1.86$ and $\kappa_{S_2 R_2} = 0.01$.

The results for $\sigma_{s_2}(q)$ has been shown in Figs. 4(e) and 4(f), from which it is evident that the slope is 1.76(2), which is compatible with the obtained result for $\nu_{s_2} \approx 2.0$. Also τ_{s_2} is obtained to be 1.31(1), which is compatible with the results of Table III. In the inset the same quantities have been calculated for R_2 yielding $\nu_{R_2} = 0.68(5)$ and $\tau_{R_2} = 3.02(0.05)$.

In addition to the mentioned exponents, we have also calculated the geometrical Green function $G(r)$ as an important quantity in 2D statistical models. It is defined as the probability that two randomly chosen points with the distance r stay on the same loop (note that this definition is different from the Green function defined commonly in sandpile models $G(|i, j|)$, which is defined as the number of toppling in site j provided that there has been a toppling in site i [21,36]). For 2D critical models, one expects that $G(r) \sim r^{-2x_l}$, x_l being the corresponding exponent. This function has been shown in Fig. 5(a) for various lattice sizes from which the power-law behavior is evident.

Let us first compare the exponents with the 2D BTW model: $\tau_s^{2DBTW} \approx 1.293$, $\tau_{S_2}^{2DBTW} = \frac{4}{3}$ and $\tau_{R_2}^{2DBTW} = \frac{5}{3}$ [4]. It is interestingly seen that $\tau_{s_2}^{2DBTW}$ lies within the statistical error bar of τ_{s_2} showing that the local properties of the effective two-dimensional system is just like the ordinary 2D BTW model, the same result as the 3D cross section in the previous section. This reveals that the local properties of the 3D and 2D cross sections are just like the 3D and 2D BTW models, respectively. The point $\tau_{s_2} > \tau_{s_2}^{2DBTW}$ arises from the fact that the probability of the formation of larger avalanche clusters in 2D cross sections is lower than 2D BTW model. This is because of the fact that in the cross sections the sand grains have the chance to leave the 2D cross section toward the extra dimensions. This reasoning is also true for R_2 . We note again that the geometrical variables (S_d and R_d in all sections, and l, r , and a in the following) have been calculated for *single component of avalanches* in a cross section not the total avalanche. The geometrical exponents of l, r, a $G(r)$ have been shown in Table IV. The data for 2D BTW and GFF models also have been shown for comparison. One may conclude that the obtained exponents are more closer to the results of GFF model.

A very different feature has been obtained for the geometrical quantities in the 2D cross section. As defined in Sec. II, after identifying the 2D avalanche clusters, we have extracted the loops, which are defined as the external frontiers of the avalanches whose lengths are named as l with gyration radius r . Also we have identified the total area simply by coloring the area inside the loop, named as a . Our analysis of l, r , and a

TABLE IV. The geometrical exponents for two-dimensional cross sections. The corresponding exponents for two-dimensional BTW [4,36] and GFF [25–27] models have also been shown for comparison.

| | τ | ν | β | $\frac{\beta}{\nu}$ | τ_{2DBTW} | τ_{2DGFF} |
|-------|-----------------|--------|---------|---------------------|-----------------------|----------------|
| l | 3.15(13) | 1.8(1) | 5.4(1) | 3.0 | 1.2 | $\frac{7}{3}$ |
| a | 2.65(12) | 2.3(1) | 5.8(1) | 2.52 | — | 2 |
| r | 4.20(11) | 1.1(1) | 4.4(1) | 4.0 | $\approx \frac{4}{3}$ | 3 |
| G_r | $x_l = 1.2(11)$ | 0.8(1) | 1.7(1) | 2.13 | Logarithmic | $x_l = 0.5$ |

contains the distribution functions and the fractal dimensions as the previous sections. The most important fractal dimension in this analysis is $\gamma_{lr} \equiv d_f$, which is known as the fractal dimension of the loops. The importance of this parameter is its relation with the other parameters in the 2D critical systems. The most important example is the diffusivity parameter (κ) in Schramm-Loewner evolution (SLE) theory. According to this theory, two-dimensional critical models are classified according to the numerical amount of κ [31], e.g., 2D BTW model belongs to $\kappa = 2$ universality class [36]. d_f and κ satisfy the relation $d_f = 1 + \frac{\kappa}{8}$ [37,38]. The results for the distribution functions have been shown in Figs. 5(b) and 5(c), and for the fractal dimensions in 5D. It is notable that, up to the maximum size considered in this paper, the fractal dimensions γ_{lr} and γ_{la} do not run with the system size L ; i.e., $\gamma_{lr}^\infty \approx \gamma_{lr}$ and $\gamma_{la}^\infty \approx \gamma_{la}$. As is seen in Table V, the exponents are very different with respect to 2D BTW model. We see that $d_f = 1.50(2)$, which is compatible with $\kappa = 4$ SLE class. This class is known to be 2D GFF [23–27]. The fractal dimensions of this model have been shown in the last row of Table V, which are very similar to the corresponding fractal dimensions of 2D cross sections, i.e., in addition to d_f , $\gamma_{S_2 R_2}^\infty = 1.86(5) \approx \frac{15}{8} = \gamma_{SR}^{GFF}$, and also $\gamma_{la} = 0.75(2) \approx \frac{3}{4} = \gamma_{la}^{GFF}$ (for more details about GFF's exponents, see Refs. [25–27]). Therefore, we conclude that although the exponents of the distribution functions of 2D GFF model is slightly different from 2D induced model, it seems that the geometrical properties of the two models are the same. This correspondence (2D cross sections of 4D BTW model and 2D GFF) should be processed and investigated more in the community to be understood more deeply, perhaps in terms of the conformal field theory.

Before closing this section, we calculate $\sigma_l(q)$ which has been presented in Figs. 5(e) and 5(f). The slope of the linear part of this figure is 1.06(7) and $\tau_l = 2.47(0.02)$. This amount differs from $\nu_l \approx 1.8$ and $\tau_l \approx 3.15$ in Table V. We note that these differences arise only for the geometrical quantities (as is also evident in the previous section), which has its roots in the multifractal behaviors of the BTW model.

At the end, we mention that the fact that $S_2^{cut} \sim L^{\nu_{s_2}}$, in which $\nu_{s_2} = 2.0$ may seem strange since if the scaling relation $S_{cutoff} \sim R_{cutoff}^{\nu_{s_2} R_d}$ holds, then one can easily find that $\nu_{s_2} = \gamma_{S_2 R_2} \nu_{R_2}$. The fact that this relation does not hold for all dimensions ($d = 2, 3$, and 4) means that the mentioned

TABLE V. The fractal dimensions for the two-dimensional cross sections. The exponents obtained from the hyper-scaling relation, i.e., Eq. (1), have also been shown for comparison. In the last row, the fractal dimensions for 2D GFF [25–27] model have also been shown which is consistent with the corresponding exponents in the 2D cross sections.

| (x, y) | (l, r) | (l, a) | (a, r) | (S_2, R_2) |
|---------------------------------|---------------|---------------|----------|----------------|
| γ_{xy}^∞ | 1.50(2) | 0.75(2) | 2.0 | 1.86(5) |
| $\frac{\tau_y - 1}{\tau_x - 1}$ | 1.50 | 0.76 | 1.97 | 1.86 |
| 2D BTW | $\frac{5}{4}$ | — | — | 2 |
| 2D GFF | $\frac{3}{2}$ | $\frac{3}{4}$ | — | $\frac{15}{8}$ |

scaling relations are modified for the scales comparable with the system size for all dimensions considered in this paper, in contrast to some previous works [4]. The decrease of S_2 due to the extra (subtracted) dimensions is more than R_2 , so that γ_{S_2, R_2} is lower than 2, which is the fractal dimension of 2D BTW avalanches.

IV. CONCLUSION

In this paper, we have considered the BTW model on its upper critical dimension $D_u = 4$. The exponents of the avalanches have been obtained using extensive numerical simulations, which are consistent with the previous results [4]. Our main concentration was upon the three and two-dimensional cross sections which were shown to be critical. It was shown that the resulting exponents in all dimensions fulfill properly the finite-size scaling relations and some hyper-scaling relations between the fractal dimensions and

the exponents of the distribution functions were shown to be valid. The number of topplings in each avalanche (s), one of the quantities which was analyzed in this paper, was shown to have the same critical properties for d -dimensional cross sections and d -dimensional BTW model. This equivalence is not true for other statistical observables which are the geometrical ones. The full information concerning the exponents have been gathered in the tables in the text. The results for the statistics of loops in the two-dimensional cross sections have been analyzed separately whose exponents are very different from the two-dimensional BTW model. We propose that the 2D cross-section properties are properly fitted to the 2D GFF. Although the exponents of the distribution functions are slightly different, the equality of the fractal dimensions is excellent. The most important exponent in this case is the fractal dimension of loops $d_f = 1.50(2)$, which is compatible with the GFF theory; i.e., $d_f^{\text{GFF}} = \frac{3}{2}$ [25–27]. The full information about the fractal dimensions has been presented in Table V.

-
- [1] P. Bak, C. Tang, and K. Wiesenfeld, *Phys. Rev. Lett.* **59**, 381 (1987).
- [2] P. Bak, C. Tang, and K. Wiesenfeld, *Phys. Rev. A* **38**, 364 (1988).
- [3] D. Sornette, *Critical Phenomena in Natural Sciences: Chaos, Fractals, Self-organization and Disorder: Concepts and Tools* (Springer Science & Business Media, Berlin, 2004).
- [4] S. Lübeck and K. D. Usadel, *Phys. Rev. E* **56**, 5138 (1997).
- [5] D. Dhar, *Physica A: Stat. Mech. Appl.* **263**, 4 (1999).
- [6] V. Priezzhev, *J. Stat. Phys.* **98**, 667 (2000).
- [7] M. De Menech and A. L. Stella, *Phys. Rev. E* **62**, R4528 (2000).
- [8] S. N. Majumdar and D. Dhar, *J. Phys. A: Math. Gen.* **24**, L357 (1991).
- [9] E. V. Ivashkevich, D. V. Ktitarov, and V. B. Priezzhev, *Physica A: Stat. Mech. Appl.* **209**, 347 (1994).
- [10] D. Dhar and S. S. Manna, *Phys. Rev. E* **49**, 2684 (1994).
- [11] D. V. Ktitarov, S. Lübeck, P. Grassberger, and V. B. Priezzhev, *Phys. Rev. E* **61**, 81 (2000).
- [12] S. Majumdar and D. Dhar, *Physica A: Stat. Mech. Appl.* **185**, 129 (1992).
- [13] S. Mahieu and P. Ruelle, *Phys. Rev. E* **64**, 066130 (2001).
- [14] H. Saleur and B. Duplantier, *Phys. Rev. Lett.* **58**, 2325 (1987).
- [15] A. Coniglio, *Phys. Rev. Lett.* **62**, 3054 (1989).
- [16] D. Dhar, *Physica A: Stat. Mech. Appl.* **369**, 29 (2006).
- [17] H. E. Stanley and N. Ostrowsky, *Random Fluctuations and Pattern Growth: Experiments and Models*, Vol. 157 (Springer Science & Business Media, Berlin, 2012).
- [18] A. Chessa, E. Marinari, A. Vespignani, and S. Zapperi, *Phys. Rev. E* **57**, R6241 (1998).
- [19] S. Lübeck, *Phys. Rev. E* **58**, 2957 (1998).
- [20] D. Marković and C. Gros, *Phys. Rep.* **536**, 41 (2014).
- [21] H. Dashti-Naserabadi and M. N. Najafi, *Phys. Rev. E* **91**, 052145 (2015).
- [22] A. A. Saberi and H. Dashti-Naserabadi, *Europhys. Lett.* **92**, 67005 (2011).
- [23] O. Schramm and S. Sheffield, *Acta Mathematica* **202**, 21 (2009).
- [24] J. Cardy, *Annals of Physics* **318**, 81 (2005).
- [25] J. Kondev and C. L. Henley, *Phys. Rev. Lett.* **74**, 4580 (1995).
- [26] J. Kondev, C. L. Henley, and D. G. Salinas, *Phys. Rev. E* **61**, 104 (2000).
- [27] J. Kondev, C. L. Henley, and D. G. Salinas, *arXiv:cond-mat/9907229* (1999).
- [28] H. N. Huynh, G. Pruessner, and L. Y. Chew, *J. Stat. Mech.: Theory Exp.* (2011) P09024.
- [29] H. N. Huynh and G. Pruessner, *Phys. Rev. E* **85**, 061133 (2012).
- [30] P. Grassberger and S. Manna, *J. Phys.* **51**, 1077 (1990).
- [31] M. N. Najafi, *Phys. Lett. A* **380**, 370 (2016).
- [32] M. N. Najafi and M. G. Nezhadhighi, *Phys. Rev. E* **95**, 032112 (2017).
- [33] S. Lübeck and K. D. Usadel, *Phys. Rev. E* **55**, 4095 (1997).
- [34] C. Tebaldi, M. De Menech, and A. L. Stella, *Phys. Rev. Lett.* **83**, 3952 (1999).
- [35] A. Chessa, A. Vespignani, and S. Zapperi, *Comput. Phys. Commun.* **121-122**, 299 (1999).
- [36] M. N. Najafi, S. Moghimi-Araghi, and S. Rouhani, *Phys. Rev. E* **85**, 051104 (2012).
- [37] M. Najafi, *Phys. Rev. E* **92**, 022113 (2015).
- [38] M. Najafi, S. Moghimi-Araghi, and S. Rouhani, *J. Phys. A: Math. Theor.* **45**, 095001 (2012).